Inorganic Chemistry

Article

pubs.acs.org/IC

Synthesis, Structure, and Magnetic Properties of $(Tb_{1-x}Mn_y)MnO_{3-\delta}$

Hao Zhang,[†] Roxana Flacau,[‡] Junliang Sun,[†] Guobao Li,*[,†] Fuhui Liao,[†] and Jianhua Lin*[,†]

[†]Beijing National Laboratory for Molecular Sciences (BNLMS), State Key Laboratory of Rare Earth Materials Chemistry and Applications, College of Chemistry and Molecular Engineering, Peking University, Beijing 100871, P.R. China

[‡]Chalk River Laboratories, Canadian Neutron Beam Centre, Chalk River, Ontario K0J 1J0, Canada

Supporting Information

ABSTRACT: Two compounds $(Tb_{1-x}Mn_y)MnO_{3-\delta}$ (W1, x = 0.089, y = 0.063; W2, x = 0.122, y = 0.102) have been synthesized by solid-state method and characterized using neutron diffraction and magnetic measurements. They crystallize in space group *Pnma* at room temperature and $Pna2_1$ at low temperature. W1 shows a sinusoidal antiferromagnetic order, and W2 shows both sinusoidal and canted commensurate antiferromagnetic orders. The magnetic moments of the commensurate antiferromagnetic order for W2 are antiferromagnetically coupled along the *a*- and *c*-axes, and ferromagnetically coupled along the *b*-axis in the $Pna2_1$ setting. Strong ferromagnetic response is induced by doping more Mn into the Tb site of $(Tb_{1-x}Mn_y)MnO_{3-\delta}$.

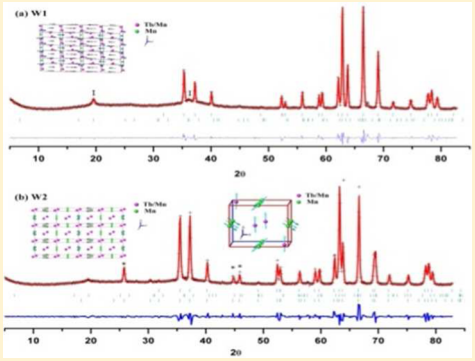

INTRODUCTION

Multiferroic materials exhibiting coexistence of two or more ferroic orders are extensively studied because of their potential applications in information storage, spintronics, and sensors.[1−8] As a result, many such materials have been reported, i.e. $TbMnO_3$,[1] $TbMn_2O_5$,[2] $BiFeO_3$,[3] CuO,[9] and $Sr_3Co_2Fe_{24}O_{41}$.[10] While most of them exhibit both antiferromagnetic and ferroelectric orders, single-phase multiferroics with both ferromagnetic and ferroelectric orders are rare.[11] It is surprising that, when a thin $TbMnO_3$ film is deposited on a substrate such as $SrTiO_3$, ferromagnetic (FM) response can be observed.[12] This phenomenon also is common to other $RMnO_3$ (R = Y, Ho, Lu) thin films,[12,13] and is proposed to arise from domain boundaries[14] or a uniform canting of an AFM spin structure.[15] On the other hand, finding this behavior in bulk multiferroics proves to be very challenging. Only recently, weak ferromagnetism was reported in bulk $Tb_{1-x}Al_xMnO_3$.[16] Similarities should be found in other doped $TbMnO_3$ compounds. Our detailed neutron diffraction and magnetic measurements presented here show that ferromagnetism occurs in our previously reported $(Tb_{1-x}Mn_y)MnO_{3-\delta}$ ($0.045 \le x \le 0.139$, $0.011 \le y \le 0.121$, and $x = 0.853y + 0.036$, $0 \le \delta$) solid solution compounds.[17]

EXPERIMENTAL DETAILS

The samples with the nominal formula $Tb_{1-x}Mn_{1+x}O_{3-\delta}$ (x = 0.0979 and 0.1358, named as W1 and W2, respectively) were synthesized from stoichiometric amounts of Tb_4O_7 (99.95%), and $MnCO_3$ (A.R.) as reported previously.[17] Powder X-ray diffraction (PXRD) data were collected on a Bruker D8 Advance diffractometer with Cu $K_{\alpha 1}$ (λ = 0.15407 nm) radiation (2θ range: 7−120°; step: 0.0197°; scan speed: 30 s/step) at 50 kV and 40 mA. Neutron powder diffraction (NPD) data were collected on the C2 High Resolution Powder Diffractometer at Canadian Neutron Beam Centre (Chalk River, Canada) with λ = 0.2370 and 0.1330 nm. The X-ray and neutron diffraction data were analyzed using GSAS[18,19] and Fullprof[20] software. The magnetic properties were investigated with a Quantum Design physical property measurement system (PPMS) from 2 to 300 K.

RESULTS AND DISCUSSIONS

The X-ray (shown in Supporting Information (SI)) and neutron diffraction patterns of W1 and W2 collected at room temperature are very similar to those previously reported.[17] Figure 1 shows the Rietveld plots of the neutron diffraction

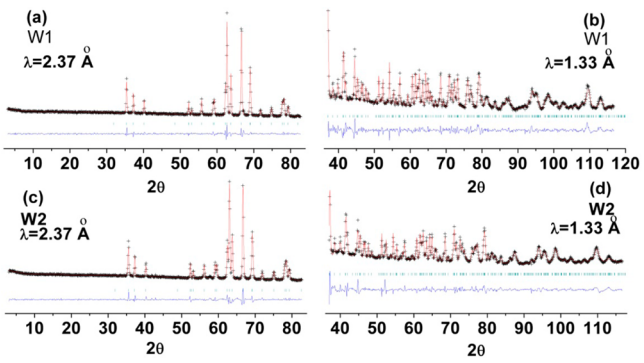

Figure 1. Rietveld plot of the neutron diffraction data for W1 (a, b) and W2 (c, d). The symbol + represents the observed value, the solid line represents the calculated value, the marks below the diffraction patterns are the calculated reflection positions, and the difference curve is shown at the bottom of the figure.

Received: January 28, 2014
Published: April 18, 2014

   dx.doi.org/10.1021/ic500222y | *Inorg. Chem.* 2014, 53, 4535−4540

data collected at room temperature, which are refined well using the corresponding structural details listed in Table 1. No

Table 1. Rietveld Refinement Details of the Neutron Diffraction Data Collected at Room Temperature for W1 and W2

	W1	W2
space group	*Pnma*	*Pnma*
lattice parameter (Å)	a = 5.7640(1), b = 7.4222(1), c = 5.2974(1)	a = 5.7268(1), b = 7.4280(1), c = 5.2953(1)
atom	x, y, z	x, y, z
Tb1/Mn1[a]	0.0766(1), 0.2500, 0.9839(1)	0.0760(1), 0.2500, 0.9841(1)
Mn2	0.0000, 0.0000, 0.5000	0.0000, 0.0000, 0.5000
O1	0.4664(1), 0.2500, 0.1041(1)	0.4654(1), 0.2500, 0.1024(1)
O2	0.3218(1), 0.0516(1), 0.7044(1)	0.3200(1), 0.0515(1), 0.7028(1)
R factor[b]	R_{wp}^{n1} = 0.042, R_{p}^{n1} = 0.031; R_{wp}^{n2} = 0.061, R_{p}^{n2} = 0.047	R_{wp}^{n1} = 0.044, R_{p}^{n1} = 0.031; R_{wp}^{n2} = 0.058, R_{p}^{n2} = 0.041

[a]The occupancy of Tb1/Mn1 is 0.911/0.063 for W1, and 0.878/0.102 for W2. [b]$R^{n1}{}_{wp}$, $R^{n1}{}_{p}$; $R^{n2}{}_{wp}$, $R^{n2}{}_{p}$ are the R factors of the whole patterns and the peaks only for neutron (n1 for λ = 2.3700 Å, and n2 for λ = 1.3300 Å) diffraction data, respectively.

reflections corresponding to impurities are found. The compositions for W1 and W2 are determined with the method reported previously[17] as $(Tb_{1-x}Mn_y)MnO_3$ with x = 0.089, y = 0.063 for W1, and x = 0.122, y = 0.102 for W2.

The temperature dependence of the magnetic susceptibilities is similar for W1 and W2, and shown in Figure 2 with two characteristic temperatures marked as T_{c1} and T_{c2} (see SI). Here, T_{c1} (T_{c2}) is the Curie temperature. The ZFC and FC curves are overlapped from the temperature T_{c1} to room temperature for both of the samples. The Curie–Weiss law is agreed well from the temperature a little above T_{c1} to room temperature:

$$\chi_p = C/(T - T_p) \quad (1\text{-}1)$$

Here χ_p is the mole magnetic susceptibility for the paramagnetic phase of the sample, C the Curie constant, T_p the Weiss constant, T the temperature. The obtained Curie constants C_{obt} for W1 and W2 are 13.83(5) and 13.44(3) emu mol^{-1} K respectively, which are close to the expected Curie constants C_{exp} (13.86 and 13.61 emu mol^{-1} K for W1 and W2 respectively) calculated by summing up the contribution of Tb^{3+}, Mn^{3+}, Mn^{4+} in the samples at high spin state. The Weiss constant T_p is −27.26(3) and −24.22(4) for W1 and W2 respectively, indicating that the interaction between the magnetic ions is antiferromagnetic.

Below T_{c1} the departure of the FC curve from the ZFC curve is the feature of the canted antiferromagnetism, which is thought to be a ferromagnetic response.[12,13] For W1, two Curie temperatures of about 22 and 37 K are observed, noted as T_{c2} and T_{c1} respectively, which are indicated in Figure 2a1. For W2, two Curie temperatures of about 30 and 42 K are found.

The magnetization curves at selected temperatures are shown in Figure 3. The M–H loops show a clear butterfly shape below 10 K for W1, and below 20 K for W2, indicating that the samples are metamagnetic at low temperature, which is similar to the reported $TbMnO_3$.[21] When the temperature increases to about T_{c2}, the M–H loops become normal, indicating that at these temperatures the reported materials are normal canted antiferromagnetic. When the temperature is above T_{c1}, the loop disappears, and the M–H curve is just a line. From Figure 3a1

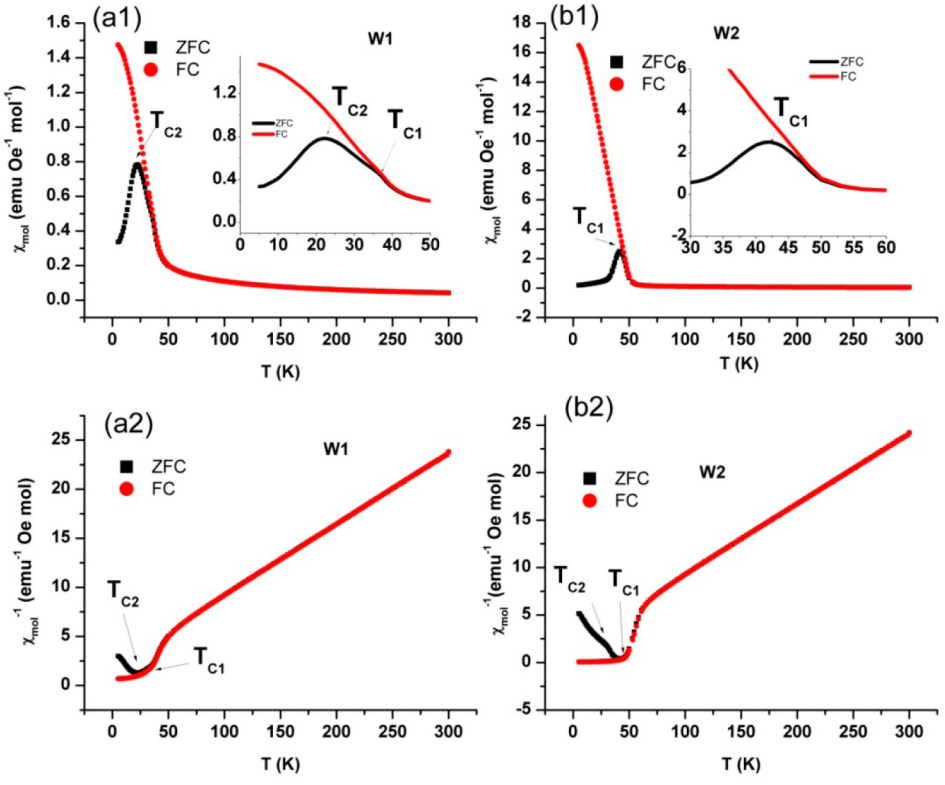

Figure 2. Temperature dependency of χ_{mol} and χ_{mol}^{-1} for W1 (a1, a2) and W2 (b1, b2).

dx.doi.org/10.1021/ic500222y | Inorg. Chem. 2014, 53, 4535–4540

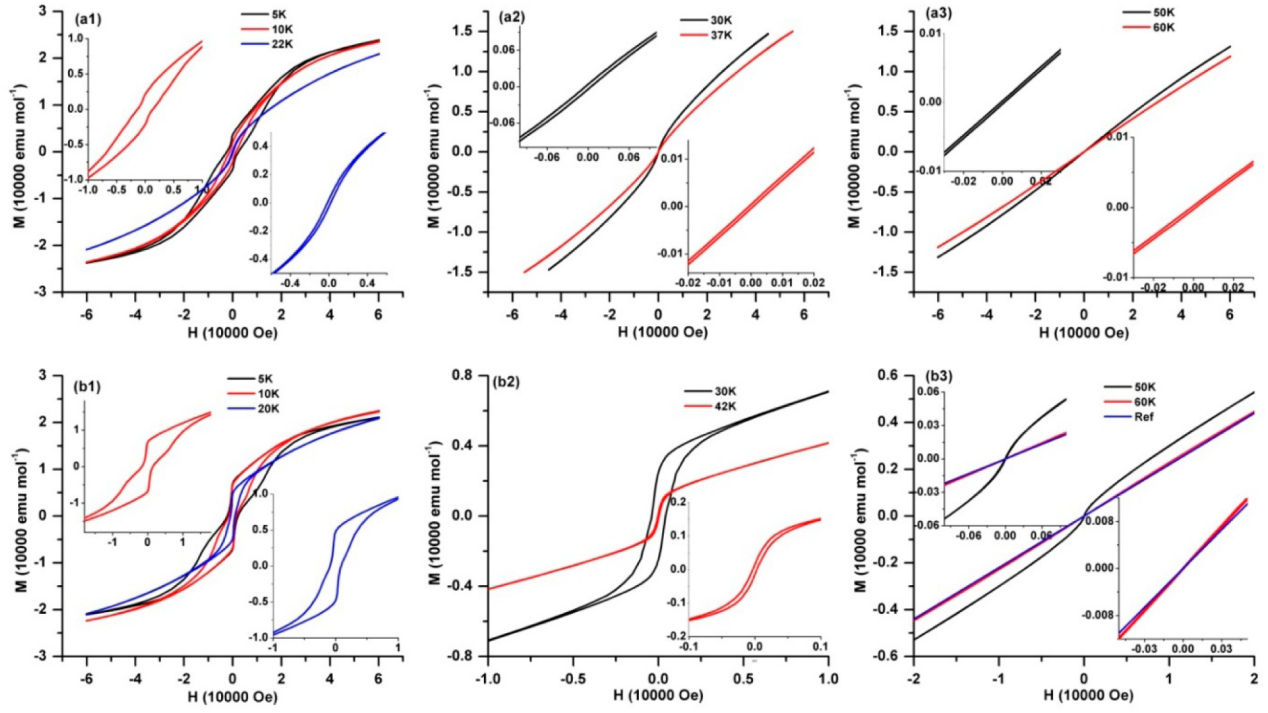

Figure 3. M−H curves at selected temperatures for W1 (a1 (5, 10, 22 K), a2 (30, 37 K), a3 (50, 60 K)) and W2 (b1 (5, 10, 20 K), b2, b3).

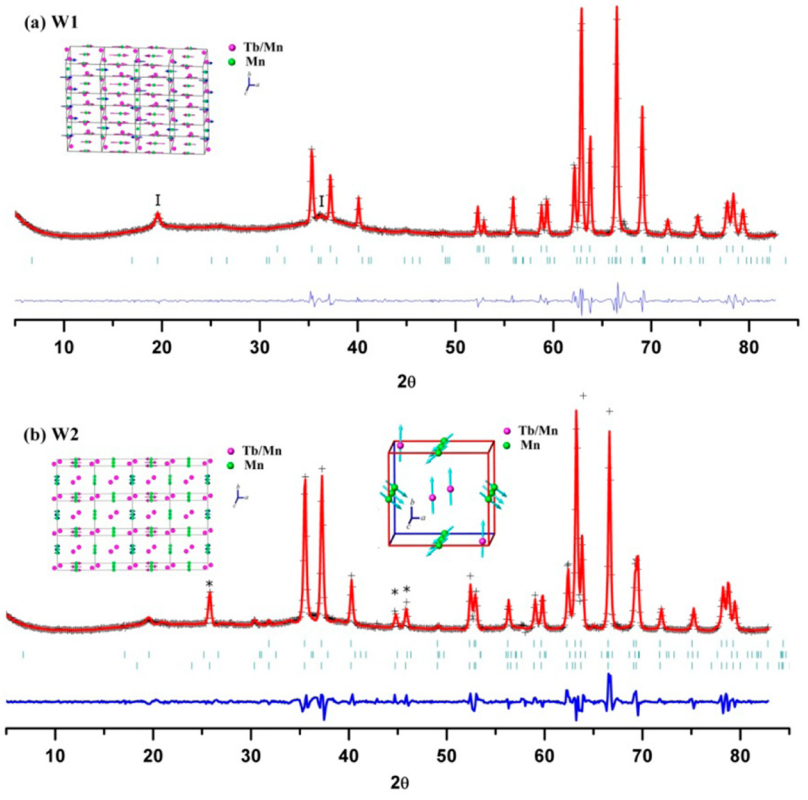

Figure 4. Rietveld plots of the neutron diffraction data for W1 (a) and W2 (b) collected at 3.5 K with λ = 2.3700 Å and analyzed using Fullprof. The symbol + represents the observed pattern, the solid line represents the calculated pattern, the marks below the diffraction patterns are the calculated reflection positions (for (a) the up and down marks are for the nuclear and magnetic diffractions, and for (b) the up, middle, and down marks are for nuclear, incommensurate antiferromagnetic, and commensurate antiferromagnetic diffractions respectively), and the difference curve is shown at the bottom of the figure. Inset is the magnetic structure used for refinement. I indicates the parent reflections caused by incommensurate antiferromagnetic ordering; * indicates the parent reflections due to commensurate antiferromagnetic ordering.

dx.doi.org/10.1021/ic500222y | Inorg. Chem. 2014, 53, 4535−4540

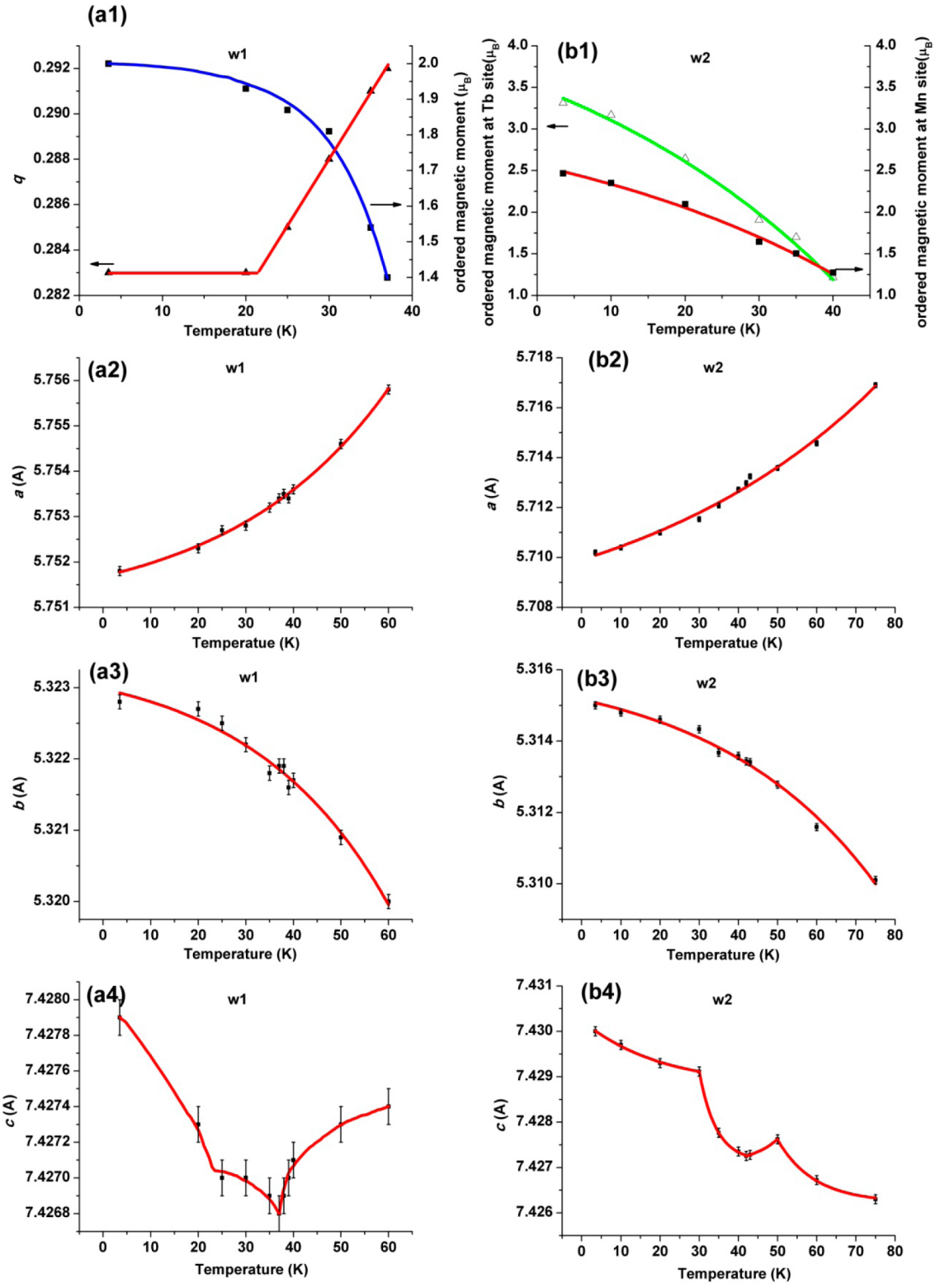

Figure 5. Temperature dependence of ordered magnetic moment, the value of q, the lattice parameters a, b, and c with error bars for W1 and W2.

and 3b1, the saturated ferromagnetic moments of nearly 5 muB per formula unit are found for W1 and W2, which is comparable to that for $TbMnO_3$.[21]

The neutron diffraction data collected at 3.5 K are shown in Figure 4 for W1 and W2. The broad reflections around 20° and 36.5° (marked with I in Figure 4a) are attributed to the sinusoidal antiferromagnetic ordering[1,22] with a wave vector $\boldsymbol{q}$ = (~0.283, 0, 0) in the space group $Pna2_1$ setting. Extra reflections around 25.7°, 44.7°, and 45.8° (marked with * in Figure 4b), appearing only in W2 can be attributed to the commensurate antiferromagntic ordering in the magnetic space group $Pn'a2_1'$. The neutron diffraction data are first refined using GSAS to obtain the lattice parameters and atoms coordinates (for W1 and W2), the magnetic moments of Tb

dx.doi.org/10.1021/ic500222y | Inorg. Chem. 2014, 53, 4535−4540

and Mn in the commensurate antiferromagnetic phase (for W2). The magnetic peaks around 20° and 36.5° are not fitted because, at present, GSAS does not include the incommensurate structures (both nuclear and magnetic). Then the software Fullprof is used to fit all the nuclear, commensurate antiferromagnetic magnetic, and the sinusoidal antiferromagnetic structures. In this case, all the parameters obtained by GSAS are used without refinement. Only the magnetic moments and the wave vector $\boldsymbol{q}$ of the sinusoidal antiferromagnetic phase are refined. Reasonably good fittings are obtained (see SI for the details) as shown in Figure 4. The wave vector q for W1 and W2 at 3.5 K are refined to be (∼0.283(1), 0, 0) in the space group $Pna2_1$ setting, which agrees well with that reported[1,22] (see SI). Following S. Quezel et al.[22] and T. Kimura et al.,[1] the wave vector $\boldsymbol{q}$ = (0.283, 0, 0) was assigned to the site of Mn during the Rietveld refinement of the neutron diffraction data, although it could be assigned to the site of Tb without decreasing the goodness of the Rietveld fitting of the diffraction data. The obtained original magnetic moments for the four Mn^{3+} ions in the unit cell at (0, 0.5, 0), (0, 0.5, 0.5), (0.5, 0, 0), and (0.5, 0, 0.5) are (M_x, 0.00, 0.00), (−M_x, 0.00, 0.00), (M_x, 0,00, 0.00), (−M_x, 0.00, 0.00) μ_B with M_x = 2.00(3) for W1 and 1.87(3) for W2, which is comparable to that reported by M. Kenzelmann et al.[23] The diffraction peaks related to the wave vector q_{Tb} = (0, 0.415, 0) reported for $TbMnO_3$ in the *Pbnm* setting was not observed.

The commensurate antiferromagnetic structure for W2 consists of two parts. One is related to the Mn site. The magnetic moments of the four Mn ions in the unit cell are coupled antiferromagnetically along the *a*- and *c*-axes, and ferromagnetically along the *b*-axis (see SI). The antiferromagnetic coupling along *a*- and *c*-axes are C- and G-types, respectively.[24] The second part is related to the Tb site. In our previous work, two kinds of atoms, Mn and Tb, are confirmed to sit at this site randomly.[17] At present, it is difficult to differentiate between the individual contribution of Tb and Mn of this site. Therefore, the total magnetic moment is considered. The magnetic moment arrangement on this site is the same as that in Mn site. However, the components along the *a*- and *c*-axes for the moment at Tb site are too small, which may be treated as zero. That is to say, the ferromagnetic coupling is the main feature of the magnetic moment on the Tb site. In addition, one may find that the ferromagnetic components of the Mn site and Tb site are coupled in an antiparallel manner. Several ABO_3 provskites allow both A and B sites to be magnetically ordered, such as $NdMnO_3$,[25] $CaMn_7O_{12}$.[26] In fact, both Tb and Mn in $TbMnO_3$ are reported to be incommensurate magnetically ordered below 7 K,[1,22] although this is not observed in our similar samples.

The magnetic reflections are similar in the diffraction data collected below T_{c1} (about 37 K) for W1. Same magnetic structure is supposed for them. Figure 5a1 shows the temperature dependence of the lattice parameters and the value of the wave vector q for W1 (see SI for the details). The value of q decreases with the decrease of temperature from 37 K to about 22 K, and seems to be constant below 22 K, which is similar to previously reported results.[1] One possible explanation for this behavior would be that W1 may be ferroelectric ordered below 22 K and thus becomes multiferroic below 22 K (more experiments are planned to confirm this). This could also explain why there is a peak at about 22 k in the χ_{mol}−T curve for W1. As expected, the ordered magnetic moment for the Mn site decreases with the increase of temperature.

When the temperature decreases, the lattice parameter *a* of W1 decreases and *b* increases. More interesting is the temperature dependence of the lattice parameter *c* shown in Figure 5a4. It first decreases from 60 K to about 37 K, after that increases to about 23 K in a flat slope and then increases to 3.5 K in a sharp slope, which may be related to the magneto−volume effect.[27] The two characteristic temperatures ∼37 K and ∼23 K agree well with the value of T_{c1} and T_{c2} for W1, respectively. This implies that this phenomenon should be magnetically related. Of course, after considering the error bars of the data obtained, the trend shown in Figure 5a4 is just for reference but not a judge. It seems very important because the electric polarization is suggested to be along the *c*-axis for $TbMnO_3$ in the $Pna2_1$ space group.[23]

The reflections corresponding to the sinusoidal antiferromagnetic ordering and the canted antiferromagntic ordering disappear in the data of W2 collected above 30 K (T_{c2}) and 42 K (T_{c1}), respectively. The ordered magnetic moment of the commensurate magnetic component, the lattice parameters *a*, *b*, and *c* of W2 at different temperatures are illustrated in Figure 5b1, 5b2, 5b3, and 5b4. It is usual that the values of the ordered magnetic moments at both Tb and Mn sites decrease when the temperature increases. The temperature dependence of the lattice parameters of W2 is similar to that of the lattice parameters of W1. The change of the lattice parameter *c* is also interesting. It first increases from 75 K to about 50 K, after that decreases to about 42 K, increases to about 30 K in a sharp slope and then further increases to 3.5 K in a flat slope. This may also be attributed to the magneto−volume effect.[27] Three characteristic temperatures, ∼30 K, ∼42 K, and ∼50 K, were found. The temperature about 30 K may be related to the disappearance of the incommensurate magnetic ordering above 30 K. The temperature about 42 K is just the T_{c1} for W2. More study should be performed to know what happens around 50 K. It may be acceptable that the unusual behavior of the lattice parameter *c* is magnetically related.

CONCLUSION

Two samples $(Tb_{1-x}Mn_y)MnO_3$ (x = 0.089, y = 0.063 for W1, and x = 0.122, y = 0.102 for W2) have been synthesized by solid-state reactions. They show similar nuclear crystal structures as $TbMnO_3$. However, the Curie temperatures for W1 ($T_{c1} \approx 37$ K, $T_{c2} \approx 22$ K) and W2 ($T_{c1} \approx 42$ K, $T_{c2} \approx 30$ K) are different from $TbMnO_3$ ($T_{N1} \approx 41$ K, $T_{N2} \approx 27$ K).[1] More interesting is that the magnetic ordering of W1 and W2 is different from that of $TbMnO_3$. $TbMnO_3$ has the sinusoidal antiferromagnetic ordering with two wave vectors $\boldsymbol{q}_{Mn}$= (∼0.283, 0, 0) and $\boldsymbol{q}_{Tb}$= (∼0.415, 0, 0) in the space group $Pna2_1$ setting below 7 K, and the sinusoidal antiferromagnetic ordering with one wave vector $\boldsymbol{q}_{Mn}$= (0.283−0.290, 0, 0) between 7 K and 41 K. W1 has the sinusoidal antiferromagnetic ordering with only one wave vector $\boldsymbol{q}_{Mn}$= (0.283−0.290, 0, 0) below 37 K. W2 has the sinusoidal antiferromagnetic ordering with one wave vector $\boldsymbol{q}_{Mn}$= (0.283−0.290, 0, 0) and commensurate canted antiferromagnetic ordering below 30 K, and only commensurate canted antiferromagnetic ordering between 30 K and 42 K. Strong ferromagnetic response is induced by doping more Mn into the Tb site of $(Tb_{1-x}Mn_y)$-$MnO_{3-\delta}$.

dx.doi.org/10.1021/ic500222y | Inorg. Chem. 2014, 53, 4535−4540

■ ASSOCIATED CONTENT

Supporting Information

The X-ray diffraction patterns, neutron diffraction data, and the refinement details at selected temperatures of W1 and W2, comments on the wave vector q for the incommensurate magnetic structure and the magnetic moment of each magnetic atom of $TbMnO_3$. This material is available free of charge via the Internet at http://pubs.acs.org.

■ AUTHOR INFORMATION

Corresponding Authors

*E-mail: liguobao@pku.edu.cn (G.L.).

*E-mail: jhlin@pku.edu.cn. Tel: (8610)62750342. Fax: (8610) 62753541 (J.L.).

Notes

The authors declare no competing financial interest.

■ ACKNOWLEDGMENTS

This work is supported by a National Key Basic Research Project of China (2010CB833103), and the National Natural Science Foundation of China (Grant 91222107).

■ REFERENCES

(1) Kimura, T.; Goto, T.; Shintani, H.; Ishizaka, K.; Arima, T.; Tokura, Y. *Nature* **2003**, *426*, 55−58.

(2) Hur, N.; Park, S.; Sharma, P. A.; Ahn, J. S.; Guha, S.; Cheong, S. W. *Nature* **2004**, *429*, 392−395.

(3) Wang, J.; Neaton, J. B.; Zheng, H.; Nagarajan, V.; Ogale, S. B.; Liu, B.; Viehland, D.; Vaithyanathan, V.; Schlom, D. G.; Waghmare, U. V.; Spaldin, N. A.; Rabe, K. M.; Wuttig, M.; Ramesh, R. *Science* **2003**, *299*, 1719−1722.

(4) Eerenstein, W.; Mathur, N. D.; Scott, J. F. *Nature* **2006**, *442*, 759−765.

(5) Rushchanskii, K. Z.; Kamba, S.; Goian, V.; Vanek, P.; Savinov, M.; Prokleska, J.; Nuzhnyy, D.; Knizek, K.; Laufek, F.; Eckel, S.; Lamoreaux, S. K.; Sushkov, A. O.; Lezaic, M.; Spaldin, N. A. K. *Nat. Mater.* **2010**, *9*, 649−654.

(6) Schmid, H. *Ferroelectrics* **1994**, *162*, 317−338.

(7) Tokura, Y. *J. Magn. Magn. Mater.* **2007**, *310*, 1145−1150.

(8) Spaldin, N. A.; Cheong, S. W.; Ramesh, R. *Phys. Today* **2010**, *63*, 38−43.

(9) Kimura, T.; Sekio, Y.; Nakamura, H.; Siegrist, T.; Ramirez, A. P. *Nat. Mater.* **2008**, *7*, 291−294.

(10) Kitagawa, Y.; Hiraoka, Y.; Honda, T.; Ishikura, T.; Nakamura, H.; Kimura, T. *Nat. Mater.* **2010**, *9*, 797−802.

(11) Hill, N. A. *J. Phys. Chem. B* **2000**, *104*, 6694−6709.

(12) Marti, X.; Skumryev, V.; Ferrater, C.; Garcia-Cuenca, M. V.; Varela, M.; Sanchez, F.; Fontcuberta, J. *Appl. Phys. Lett.* **2010**, *96*, 222505.

(13) White, J. S.; Bator, M.; Hu, Y.; Luetkens, H.; Stahn, J.; Capelli, S.; Das, S.; Dobeli, M.; Lippert, T.; Malik, V. K.; Martynczuk, J.; Wokaun, A.; Kenzelmann, M.; Niedermayer, C.; Schneider, C. W. *Phys. Rev. Lett.* **2013**, *111*, 037201.

(14) Daumont, C. J. M.; Mannix, D.; Venkatesan, S.; Catalan, G.; Rubi, D.; Kooi, B. J.; De Hosson, J. T. M.; Noheda, B. *J. Phys.: Condens. Matter* **2009**, *21*, 182001.

(15) Marti, X.; Skumryev, V.; Laukhin, V.; Bachelet, R.; Ferrater, C.; Garcia-Cuenca, M. V.; Varela, M.; Sanchez, F.; Fontcuberta, J. J. *Appl. Phys.* **2010**, *108*, 123917.

(16) Astudillo, A.; Izquierdo, J.; Bonilla, F. J.; Bolaños, G.; Morán, O. *IEEE Trans. Magn.* **2013**, *49*, 4590−4593.

(17) Wang, R.; Yang, C. X.; Fan, M.; Wu, M. M.; Wang, C. H.; Yu, X. H.; Zhu, J. L.; Zhang, J. R.; Li, G. B.; Huang, Q. Z.; Chen, D. F.; Jin, T. N.; Kamiyama, T.; Liao, F. H.; Lin, J. H. *J. Alloy. Compd.* **2013**, *554*, 385−394.

(18) Rietveld, H. M. *J. Appl. Crystallogr.* **1969**, *2*, 65−71.

(19) Vegard, L. *Z. Phys.* **1921**, *5*, 17−26.

(20) Rodriguez-Carvajal, J. *Physica B* **1993**, *12*, 55−69.

(21) Kimura, T.; Lawes, G.; Goto, T.; Tokura, Y.; Ramirez, A. P. *Phys. Rev. B* **2005**, *71*, 224425.

(22) Quezel, S.; Tcheou, F.; Rossatmignod, J.; Quezel, G.; Roudaut, E. *Physica B and C* **1977**, *86*, 916−918.

(23) Kenzelmann, M.; Harris, A. B.; Jonas, S.; Broholm, C.; Schefer, J.; Kim, S. B.; Zhang, C. L.; Cheong, S. W.; Vajk, O. P.; Lynn, J. W. *Phys. Rev. Lett.* **2005**, *85*, 087206.

(24) Wollan, E. O.; Koehler, W. C. *Phys. Rev.* **1955**, *100*, 545−563.

(25) Muñoz, A.; Alonso, J. A.; Martinez-Lope, M. J.; Garcia-Munoz, J. L.; Fernandez-Diaz, M. T. *J. Phys.: Condens. Matter* **2000**, *12*, 1361−1376.

(26) Johnson, R. D.; Chapon, L. C.; Khalyavin, D. D.; Manuel, P.; Radaelli, P. G.; Martin, C. *Phys. Rev. Lett.* **2012**, *108*, 067201.

(27) Diop, L. V. B.; Amara, M.; Isnard, O. *J. Phys.: Condens. Matter* **2013**, *25*, 416007.